

15. ORGANIC MATTER AND CARBON ISOTOPE COMPOSITION OF CARBONATE NODULES AND ASSOCIATED SEDIMENTS FROM MIDDLE VALLEY, LEG 139¹

M. Boni,² B.R.T. Simoneit,³ G.L. Früh-Green,⁴ R.N. Leif,³ and J.A. McKenzie⁴

ABSTRACT

Carbonate nodules and associated sediments from Ocean Drilling Program Leg 139 sites of the Middle Valley, Juan de Fuca Ridge, were studied using a combination of inorganic and organic geochemical techniques. The mineralogy and stable isotopic compositions defined three types of nodules, reflecting the conditions of carbonate precipitation. Nodule ingrowth has entrapped the sedimentary organic matter, and concomitant displacement of the sedimentary mineral matrix and associated organic matter resulted in decreased bitumen extract yields from the nodules. Molecular organic geochemical analyses of the bitumen by gas chromatography-mass spectrometry revealed that polycyclic aromatic hydrocarbons are major constituents in the total extracts, reflecting the high-temperature origin of the entrapped hydrothermal organic products. Strong reducing conditions are evident during the hydrothermal alteration of biomarker precursors to products. The oxygen isotope data reflect the lower fluid temperatures during carbonate precipitation.

INTRODUCTION

Numerous detailed geophysical studies (e.g., Davis, Goodfellow, et al., 1987), as well as geochemical analyses from shallow piston cores (e.g., Goodfellow and Blaise, 1988), carried out during the last 10 years in order to define the structural and thermal setting in Middle Valley, Juan de Fuca Ridge, have been the premise for more intensive research in this area. This was performed during Ocean Drilling Program (ODP) Leg 139 (Davis, Mottl, Fisher, et al., 1992). Four sites with distinctly variable heat flow, sediment thickness, and igneous rock type were drilled during this leg (Davis, Mottl, Fisher, et al., 1992). The sites, defined mostly on the basis of their hydrologic conditions, are as follows: Site 855, an area of fluid recharge at lower temperatures; Site 856, an area of fossil discharge where important deposits of massive sulfides have been discovered; Site 857, a hydrothermal reservoir; and Site 858, an area of active discharge. At Sites 856–858, the cored clastic sedimentary sequences showed strong modifications induced by hydrothermal activity. These modifications can be documented not only by the petrographical, mineralogical, and geochemical compositions of the authigenic mineral phases, but also in the characteristics and distribution of the organic compounds throughout the clastic sediments at various levels of diagenesis and catagenesis (Davis, Mottl, Fisher, et al., 1992).

Among the various authigenic phases recognized in the sediments cored in Middle Valley, the most obvious are the carbonate nodules and concretions recovered at several depths from Sites 856, 857, and 858. Similar carbonate concretions of various shapes, impregnating both hemipelagic and turbiditic shallow sediments (<10 mbsf), have been described from the same area (Goodfellow and Blaise, 1988; Al-Aasm and Blaise, 1991). This volume contains other papers describing the mineralogy and geochemistry, including isotope geochemistry, of the carbonate concretions (Baker et al.; Buatier et al.; Früh-Green et al.; Leybourne and Goodfellow, this volume). Deposition of carbonate

concretions is considered a distal effect of the higher temperature hydrothermal activity in the whole area.

This paper is an exploratory contribution on the composition of the solvent extractable organic content in carbonate nodules coupled with their stable isotope geochemistry. We hope to further define the nature and origin of carbon in both early and/or late diagenetic carbonates in hydrothermally affected sediments.

GEOLOGICAL SETTING AND DESCRIPTION OF SITES

Middle Valley is a fault-bounded rift valley located at the northern extremity of the Juan de Fuca Ridge, just south of the Sovanco fracture zone. Its geological setting was first described by Davis, Currie, and Kosalos (1987) and, more recently, by Davis and Villinger (1992). The sedimentary sequence filling the valley generally consists of turbidite units interbedded with pelagic sediments, with a thickness ranging from 300 to 1500 m. The elevated basement temperatures recorded in the valley (100°–300°C at hole bottoms, Davis and Villinger, 1992) probably reflect the high thermal insulating capacity and low permeability of the sedimentary sequence, which plays an important role in maintaining high fluid temperatures and facilitating hydrothermal discharge at a restricted number of vent sites (Goodfellow and Blaise, 1988). Heat flow in the valley sediments seems to be inversely correlated with their thickness (Davis and Villinger, 1992).

Among the sedimentary sequences cored in Middle Valley during Leg 139, only Sites 856, 857, and 858 were strongly affected by hydrothermal activity, as reflected among other evidence, by the deposition of carbonate nodules. Therefore, we will refer in this study only to these sites, and especially to Site 858, situated in the middle of an actively venting field (Davis, Mottl, Fisher, et al., 1992).

Site 856

Site 856 is located in the eastern part of Middle Valley (Fig. 1). It is about 3 km west of the normal fault scarp forming the eastern topographic boundary of the valley, on a small circular hill (Bent Hill) that has a diameter of about 500 m and stands 60 m above the floor. There is no heat flow anomaly associated directly with the hill; it appears to be thermally extinct (Davis and Villinger, 1992). At this site the carbonate concretions occur only in Hole 856A, stratigraphic subunit IIA (Davis, Mottl, Fisher, et al., 1992), from about 30 to 110 mbsf, and are mostly related to turbidite lithology. Examples are shown in Figure 2A (at 9 and 19 cm).

¹ Mottl, M.J., Davis, E.E., Fisher, A.T., and Slack, J.F. (Eds.), 1994. *Proc. ODP, Sci. Results, 139*: College Station, TX (Ocean Drilling Program).

² Dipartimento di Scienze della Terra, Università degli Studi di Napoli 'Federico II', Largo S. Marcellino 10, 80138 Naples, Italy.

³ College of Oceanic and Atmospheric Sciences, Oregon State University, Corvallis, OR 97331, U.S.A.

⁴ Geologisches Institut, Eidgenössische Technische Hochschule, 8092 Zürich, Switzerland.

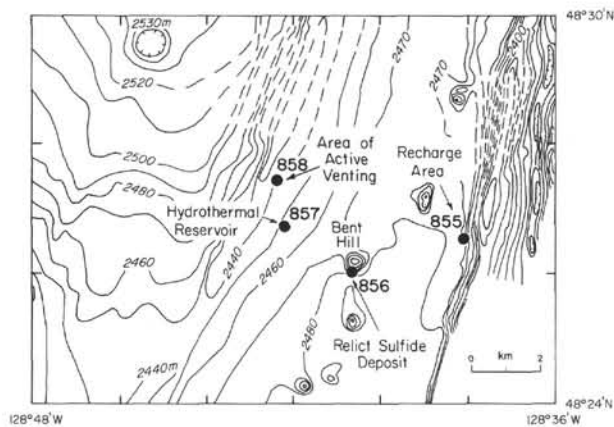


Figure 1. Location map of Leg 139 drill sites in Middle Valley, northeast Pacific. Bathymetry in meters.

Site 857

Site 857 is located 5.2 km west of the normal fault scarp of the valley and 1.5 km east of the fault that forms the current structural boundary of the central rift (Fig. 1). It is also situated 2 km south of the active vent area cored at Site 858 (Davis, Mottl, Fisher, et al., 1992). The site is situated over a buried basement fault block standing 1 km above the normal basement level of the valley. A major thermal anomaly exists here over an area extending more than 10 km in length in a rift-parallel direction, even though no fluid discharge activity has been recorded (Davis and Villinger, 1992). At this site, carbonate concentrations are generally in the form of cement in the clastic sediments, as well as in small veins and fracture fillings. They occur particularly in Holes 857A and 857C, stratigraphic subunits IIA and IIB (Davis, Mottl, Fisher, et al., 1992), at depths ranging from 75 to at least 350 mbsf.

Site 858

Site 858 is located in the middle of an active, 800-m-long and 400-m-wide venting area, 1.8 km north of Site 857 and about 6 km east of the present axis of the rift valley (Fig. 1). The vent field is situated over a local basement high, and the sediment thickness in the area ranges from 400 to 700 m (Davis, Mottl, Fisher, et al., 1992). Fluids discharge at temperatures between 255° and 275°C through numerous scattered vents. Heat flow in the area surrounding the vent field decreases systematically with distance from the field, falling to background levels over a distance of a few hundred meters (Davis and Villinger, 1992). At this site, carbonate nodules and concretions have been recovered from Holes 858A, 858C, 858D, and 858F in lithologic units I and II (Davis, Mottl, Fisher, et al., 1992), at depths ranging from about 10 to 100 mbsf. An example is shown in Figure 2B (24–30 cm).

METHODS

The nodules and the soft-sediment samples were studied in thin section, both under normal and cathodic light, to determine their petrographic characteristics and the distribution of carbonates. A Technosyn 8200 MKIII cold cathode, with a beam voltage of 15 kV and a current of 200 μ A was used for cathodoluminescence. This part of the analyses was performed at the University of Naples. At the ETH-Zürich the nodules were analyzed further with a five spectrometer CAMECA SX 50 electron microprobe, using both wavelength-dispersion and energy-dispersion modes. The acceleration voltage was 15 kV and the beam current about 15 μ A. Also at the ETH the carbonate mineralogy was determined by bulk X-ray diffraction (XRD) analysis on a Scintag X-ray diffractometer. Carbon and oxygen isotope ratios

of carbonates were determined on both soft and indurated sediments, as well as on carbonate nodules (Früh-Green et al., this volume). CO_2 gas for isotopic analysis was prepared from the carbonates by reaction with phosphoric acid (McCrea, 1950). The phosphoric acid correction factor of 1.01025 for calcite was applied (Sharma and Clayton, 1965). The isotopic ratios were determined by conventional mass spectrometric analysis and are reported in the δ notation (per mil, ‰) relative to the PDB isotopic standard for carbonates. The overall reproducibility for carbonates is $\pm 0.2\text{‰}$.

Temperatures have been estimated from oxygen isotope data by applying experimentally determined fractionation factors for calcite-water (O'Neil et al., 1969, as reported in Friedman and O'Neil, 1977) and considering two cases for the oxygen isotope composition of the hydrothermal fluid (Table 1). In the first case, an unaltered seawater oxygen isotope composition of 0.00‰ relative to the Standard Mean Ocean Water (SMOW) standard is assumed. In the second case, an altered seawater composition, with an average $\delta^{18}\text{O}$ value of 2‰ is applied. This latter value is based on results of Früh-Green et al. (this volume), who suggest that the hydrothermal fluids were shifted towards positive $\delta^{18}\text{O}$ values between 1‰ and 5‰. The $\delta^{18}\text{O}$ values of calcite on the Pee Dee Belemnite (PDB) and SMOW scales are related by the expression: $\delta^{18}\text{O}_{\text{SMOW}} = 1.03086 \delta^{18}\text{O}_{\text{PDB}} + 30.86$ (Friedman and O'Neil, 1977).

For organic geochemical analyses at Oregon State University, the nodule or sediment samples were gently ground in an agate mortar, and a known amount (0.5–3 g) transferred into screw-capped vials for extraction. Hexane (2 mL) and methanol (1 mL) were added and the suspension heated at 60°C in a water bath and shaken occasionally for about two hours. After centrifuging, the clear supernatant solution was pipetted into a second vial and the extraction was repeated with another 1 mL aliquot of hexane. Combined extracts were evaporated under nitrogen blow-down at 30°C to volumes of 10 to 40 μ L. A 1- to 3- μ L sample was then injected onto the gas chromatograph (GC) or GC-mass spectrometer (MS) using normal protocol. Hydrocarbons were identified by comparison of the retention times with those of authentic standards and confirmation by GC-MS. The final quantification of the results on total hexane soluble matter is based on the weight of dry sediment and the aliquot used in the injection.

The GC is a Hewlett-Packard Model 5890A, fitted with a 30 m \times 0.25 mm capillary column coated with DB-5 (0.25 μ m film thickness). The GC oven temperature was programmed at isothermal for 2 min at 65°C, 4°C/min to 310°C, and isothermal for 30 min, with the injector at 290°C, flame ionization detector (FID) at 325°C, and helium as the carrier gas.

Analyses by GC-MS were carried out with a Finnigan Model 9610 gas chromatograph coupled to a Finnigan Model 4021 quadrupole mass spectrometer operated at 70 eV over the mass range 50–650 dalton. The GC was fitted with an identical column to that above for the analytical GC, and the same temperature program and operating conditions as above were used. The GC-MS data were acquired and processed with an on-line Finnigan-Incos Model 2300 computer data system. Compounds were identified from GC retention times, comparison with authentic standards, literature data and interpretation of mass spectrometric fragmentation patterns.

The total C, N, and S analyses were carried out at Oregon State University with a Carlo Erba NA 1500 CNS analyzer by combustion of bulk samples to 1000°C and measurement of the gases by GC.

RESULTS AND DISCUSSION

Only a few nodules have been analyzed for their organic matter in this preliminary paper, and among these, one concretion (Sample 858B-2H-3, 126–129 cm) consists of gypsum and anhydrite cementing fine silty sediment, which was analyzed for its elemental composition only. The stable isotope data and elemental (C, N, S) analyses are given in Table 1 and the lipid/bitumen yields and parameters are found in Table 2.

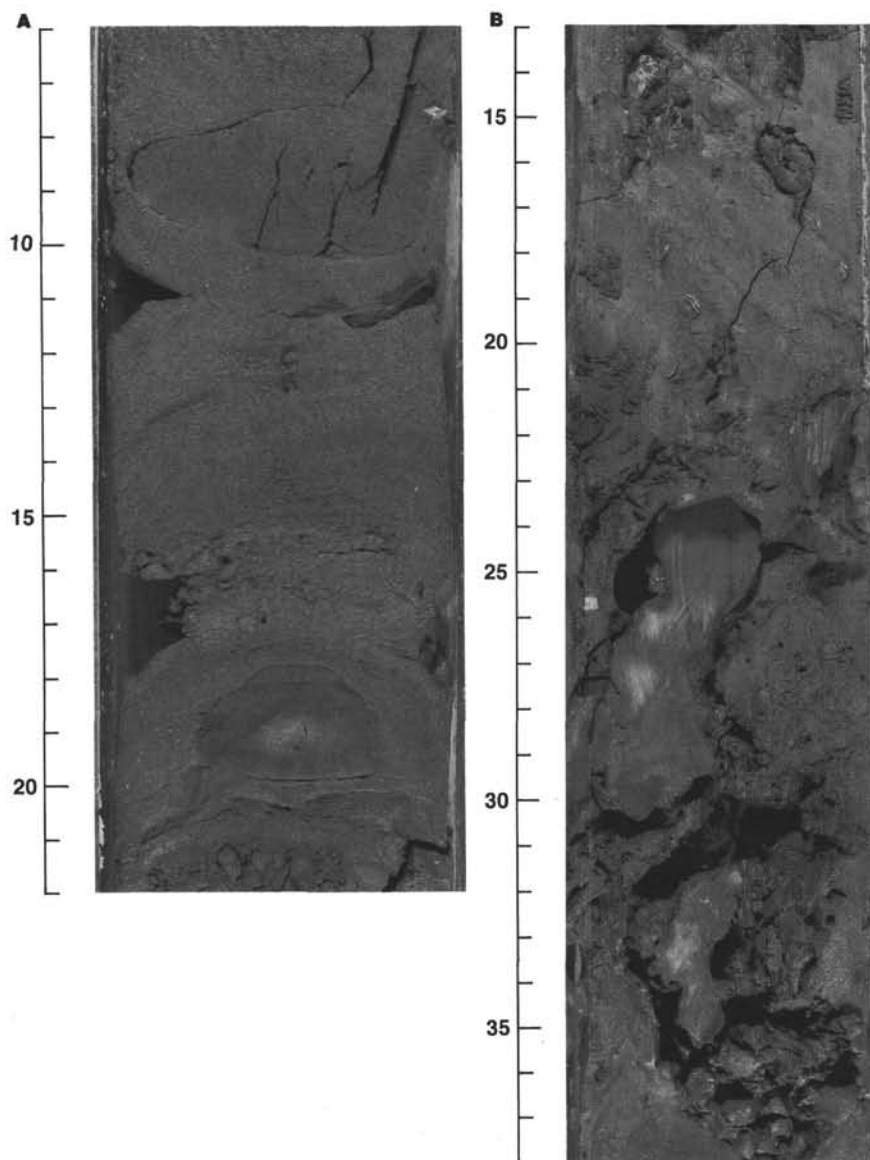


Figure 2. Photographs of core sections showing nodules and sediment matrix. **A.** Sample 856A-10X-3CC, 6–22 cm, carbonate nodules (calcite) growing in a poorly cemented, coarse silty, turbiditic unit. **B.** Sample 858A-2H-7, 13–38 cm, carbonate nodules (calcite) growing in fossiliferous, hemipelagic, silty clay.

Site 856

Nodules

Only two samples, 856A-6H-4, 18–22 cm (45.4 mbsf), and 856A-6H-4, 73–76 cm (45.9 mbsf), were analyzed from this site for both stable isotopes and organic matter. The first consists of poorly calcite-cemented soft mud, the second of well-indurated coarse silt with cross lamination and pyrite. This latter nodule is rounded and does not appear to be diagenetically zoned. Microprobe analysis on selected points of the carbonate cement of the nodule showed the presence of low-Mg calcite, with an average Mn content higher than 1 wt%.

Both the scarce calcite cement of the soft sediments and the nodule calcite show depletions in ^{13}C as well as in ^{18}O , relative to normal marine carbonates (Table 1). Large differences exist, however, in both carbon and oxygen isotope compositions between the two samples, possibly recording quite distinct conditions of carbonate precipitation (see Früh-Green et al., this volume). Changes in conditions of carbonate precipitation are particularly evident from the isotopic profile measured on microsamples that were drilled across a 2-cm-thick nodule at 45.93 mbsf (856A-6H-4, 73–76 cm). The systematic variation of increasing $\delta^{13}\text{C}$ and decreasing $\delta^{18}\text{O}$ observed from the center

to the rim (Table 1) indicates a change in temperature and/or isotopic composition of the precipitating fluid during growth of the nodule. The $\delta^{13}\text{C}$ values of the two samples investigated here lie within the general range of carbon isotope compositions of calcite cements and nodules from Hole 856A (Früh-Green et al., this volume). Low $\delta^{13}\text{C}$ values are typical of carbonate nodules in the Middle Valley sediments (e.g., Al-Aasm and Blaise, 1991) and indicate the incorporation of carbonate ions derived from organic matter. The ^{13}C depletion recorded in the carbonates reflects the incorporation of carbonate ions derived from organic matter by: (1) sulfate reduction reactions, in which organic matter is oxidized by bacterial and/or thermochemical processes to produce bicarbonate (HCO_3^-) hydrogen sulfide (H_2S), and/or ammonia (NH_3); or (2) from thermal decomposition of organic matter in the absence of sulfate at high temperatures (e.g., Machel, 1987; Raiswell, 1987).

Bitumen

The total carbon (TC) content of the samples from Hole 856A is 0.53% in the sediment compared to 2.34% in the nodule (Table 1) and the bitumen yield is high with respect to the nodule (Table 2). The hydrocarbons are composed of traces of normal alkanes with carbon

Table 1. Sample descriptions, isotopic, and elemental compositions of nodules and sediments from Leg 139.

Sample	Sub-bottom depth (mbsf)	Description	Cement mineralogy	Carbonate				Carbon (Total, %)	Nitrogen (Total, %)	Sulfur (Total, %)
				$\delta^{13}\text{C}$ (‰, PDB)	$\delta^{18}\text{O}$ (‰, PDB)	Temp. calc. (°C) ¹				
						a (0‰)	b (2‰)			
856A-6H-4, 18-22	45.4	Soft mud	Calcite	-9.89	-14.77	114	137	0.53	0.03	0.11
856A-6H-4, 73-76	45.9	Nodule	Calcite	-20.01	-9.62	68	84	2.34	0.03	0.09
		Profile: rim		-18.53	-11.14	80	97			
		Rim to center		-20.39	-8.88	63	78			
		Center		-21.07	-8.36	59	74			
		Rim to center		-22.05	-11.01	79	86			
		Rim		-20.83	-9.45	67	82			
857C-36R-1, 50-53	346.5	Nodule	Calcite	-12.73	-19.72	182	220	0.18	0.03	0.33
858A-2H-7, 40-42	11.8	Nodule	Calcite	-31.79	+3.56	-1	7	0.68	0.05	0.74
858A-4H-7, 15-17	30.6	Nodule	Calcite	-9.31	-17.08	142	170	1.45	0.05	2.21
858A-8H-2, 57-59	61.0	Nodule	Calcite	-11.10	-12.02	88	106	6.88	0.10	0.26
		Sediment						1.19	0.05	
858B-2H-3, 126-129	11.5	Breccia	Anhydrite + Gypsum					0.13	<0.02	17.40
858C-2H-5, 71-73	10.3	Nodule	Calcite	-24.19	-1.28	20	29	8.60	0.03	0.12
		Sediment	Calcite-rich	-9.50	-7.92	57	70	0.73	0.04	1.41
858C-3H-2, 110-115	15.5	Breccia	Calcite	-22.76	-10.70	77	93	10.50	0.03	0.90
858D-4H-1, 5-7	19.9	Nodule	Calcite					6.29	0.04	0.12
		Profile: rim		-17.61	-6.88	50	63			
		Rim to center		-17.41	-7.04	51	64			
		Rim		-17.31	-6.70	49	61			
858F-2R-CC, 0-5	37.2	Nodule	Calcite	-27.78	+2.53	3	11			

¹Temperatures estimated from calcite-water fractionations, assuming: (a) an unaltered seawater $\delta^{18}\text{O}$ value of 0‰ (SMOW), and (b) an altered value of 2‰ (cf. Früh-Green *et al.*, this volume).

Table 2. Lipid/bitumen composition and parameters of nodules and sediments from Leg 139.

Sample	Sub-bottom depth (mbsf)	Description	Bitumen yield ($\mu\text{g/g}$ dry wt.)	Hydrocarbon parameters				Biomarker parameters	
				n -Alkanes CPI ₂₆₋₃₅ ¹	Pr/Ph ²	Pr/ n -C ₁₇	Ph/ n -C ₁₈	C ₃₂ triterpanes $\left(\frac{S}{S+R}\right)$	C ₂₉ steranes $\left(\frac{20S}{20S+20R}\right)$
856A-6H-4, 18-22	45.4	Mud	22.3	—	—	—	—	—	—
856A-6H-4, 73-76	45.9	Nodule	2.1	0.85	—	—	—	—	—
		Sediment	8.7	0.81	—	—	—	—	—
857C-36R-1, 50-53	346.5	Concretion	17.3	—	—	—	—	—	—
858A-2H-7, 40-42	11.8	Nodule	3.4	3.60	0.60	0.86	1.30	—	—
		Sediment	4.1	4.90	0.89	0.80	1.10	—	—
858A-4H-7, 15-17	30.6	Nodule	12.4	0.82	0.70	0.20	0.24	—	—
858A-8H-2, 57-59	61.0	Nodule	5.2	0.92	—	—	—	—	—
		Sediment	10.8	0.94	—	—	—	—	—
858C-2H-5, 71-73	10.3	Nodule	—	1.50	1.27	0.42	0.73	0.29	—
		Sediment	—	1.74	1.13	0.36	0.86	0.25	—
858C-3H-2, 110-115	15.5	Breccia	5.2	0.62	0.33	1.60	1.80	0.60	0.39
		Sediment	30.3	0.63	0.29	2.10	2.40	0.56	0.41
858D-4H-1, 5-7	19.9	Nodule	26.1	0.87	0.32	0.19	2.94	0.43	0.15

¹ CPI = carbon preference index, i.e., sum of odd to sum of even n -alkanes from C₂₆ to C₃₅.

² Pr = pristane, Ph = phytane, — = below detection limit.

preference indexes (CPI) of 0.85 and 0.81 for sediment and nodule (Table 2), polynuclear aromatic hydrocarbons (PAH) at significant concentrations, and biomarkers such as triterpanes and steranes are not detectable.

The major PAH are shown in Figures 3A and 4A and the various molecular ratios are given in Table 3. The dominant PAH is phenanthrene with successively lesser concentrations of fluoranthene, pyrene, chrysene/triphenylene, benzofluoranthenes, benzo(e)pyrene, benzo(a)pyrene, indeno(1,2,3-cd)perylene, and coronene. Perylene is present as a trace component only. The presence of the analogs with a five-membered alicyclic ring (e.g., benzofluoranthenes, indeno(1,2,3-cd)perylene), as well as the other peri-condensed aromatic hydrocarbons, confirms the high-temperature origin of these PAH (Simoneit and Lonsdale, 1982; Blumer, 1975; Scott, 1982; Simoneit, 1984).

The low level of perylene and the PAH indexes indicate significant maturity for these samples. The traces of alkanes and the dominance of the PAH support the interpretation that this sedimentary section was subjected to hydrothermal fluid invasion in excess of 200°–250°C prior to nodule formation, which removed the alkanes and brought in or generated the PAH. The low bitumen concentration in the nodule vs. the surrounding sediment reflects the dilution of the matrix and associated organic matter by carbonate precipitation/growth.

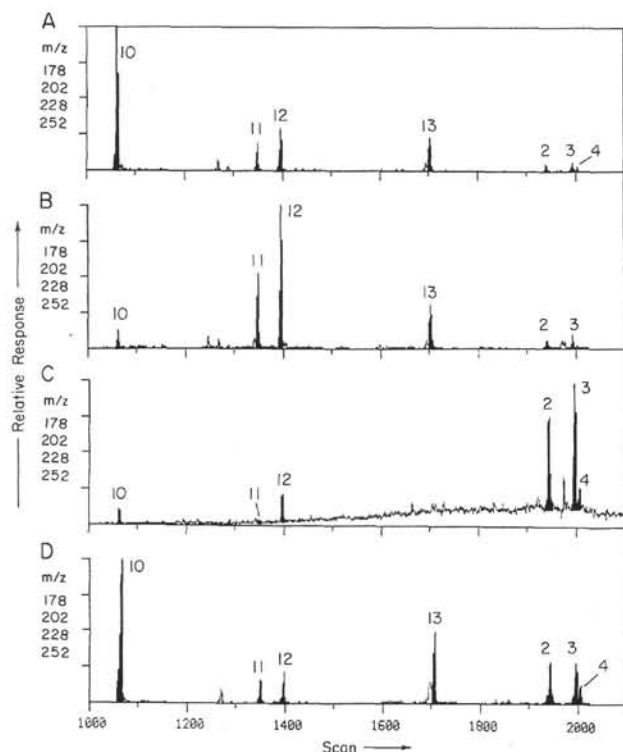


Figure 3. Summed mass fragmentograms (total ion current for m/z 178, 202, 228, and 252) for selected PAH in total bitumen of Samples 856A-6H-4, 18–22 cm (A), 858A-4H-7, 15–17 cm (B), 858D-4H-1, 5–7 cm (C), and 857C-36-1, 50–53 cm (D) (10 = phenanthrene, 11 = fluoranthene, 12 = pyrene, 13 = chrysene/triphenylene, 2 = benzofluoranthenes, 3 = benzo(e)pyrene, 4 = benzo(a)pyrene).

Site 857

Nodule

A single concretion has been examined from this site (Sample 857C-36R-1, 50–53 cm). It fills a fracture at considerable depth (346.5 mbsf). This nodule consists of calcite and has a relatively low (0.5 wt% Mn) Mn content.

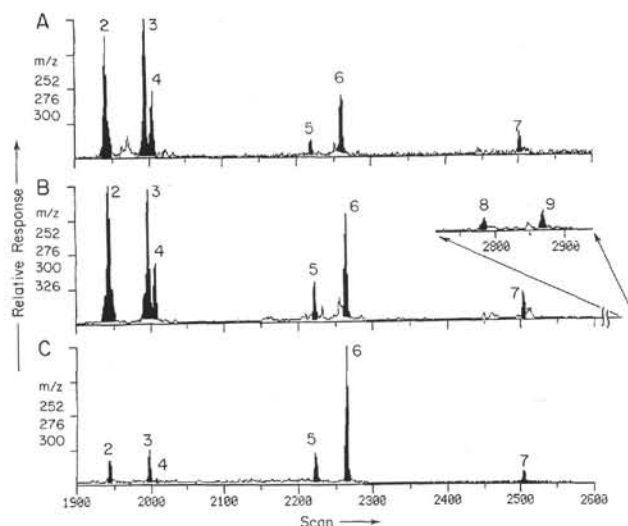


Figure 4. Summed mass fragmentograms (total ion current for m/z 252, 276, 300, and 326) for selected PAH in total bitumen of Samples 856A-6H-4, 18–22 cm (A), 857C-36R-1, 50–53 cm (B), and 858D-4H-1, 5–7 cm (C) (2 = benzofluoranthenes, 3 = benzo(e)pyrene, 4 = benzo(a)pyrene, 5 = indeno(1,2,3-cd)pyrene, 6 = benzo(ghi)perylene, 7 = coronene, 8 and 9 = unknowns m/z 326).

The isotopic values of the carbonate are quite depleted in both ^{13}C and ^{18}O (Table 1). In this nodule, a precipitation temperature of 182°C has been calculated, which is much lower than the temperature estimated during the leg at the same depth in Hole 857C (246°C) based on a 0.71°C/m geothermal gradient. The $\delta^{13}\text{C}$ value is -12.73‰ , possibly resulting from both oxidation reactions of organic matter by sulfate and thermal decarboxylation at depth during catagenesis.

Bitumen

The TC content of this nodule is low (0.18%, Table 1), although the bitumen yield is significant (Table 2). Normal alkanes and biomarkers such as triterpanes and steranes are not detectable due to their low concentration relative to the dominant PAH (Table 3). The major PAH are shown in Figures 3D and 4B, and the various molecular ratios are given in Table 3.

Table 3. Maturity parameters of aromatic hydrocarbons in Leg 139 nodules and sediments.

Sample	Description	Phenanthrene series ¹			Fluoranthene/ pyrene	Perylene/ benzofluoranthenes + BaP + BeP	BaP/BeP	Coronene/ BaP + BeP + Bzfl.
		P/MP	MPI 1	MPI 2				
856A-6H-4, 18-22	Mud	15.0	0.05	0.05	0.70	0.11	0.47	0.07
856A-6H-4, 73-76	Nodule	6.58	0.13	0.15	0.68	—	0.18	—
857C-36R-1, 50-53	Concretion	1.74	0.66	0.80	0.77	0.007	0.44	0.8
858A-2H-7, 40-42	Nodule	—	—	—	0.38	35.0	—	—
	Sediment	2.09	0.30	0.35	1.13	26.7	—	—
858A-4H-7, 15-17	Nodule	0.36	2.35	2.82	0.50	0.027	0.20	0.09
858A-8H-2, 57-59	Nodule	6.27	0.05	0.04	0.59	0.037	0.25	—
858C-2H-5, 71-73	Nodule	—	—	—	0.10	< 0.02	0.04	0.69
	Sediment	—	—	—	0.22	< 0.02	0.03	0.56
858C-3H-2, 110-115	Breccia	—	—	—	0.35	0.017	0.12	2.18
	Sediment	—	—	—	0.40	0.019	0.05	2.04
858D-4H-1, 5-7	Nodule	1.26	0.77	0.95	0.14	0.01	0.15	0.18

¹P/MP = phenanthrene/methylphenanthrenes, $\text{MPI 1} = \frac{1.5(3\text{MP} + 2\text{MP})}{\text{P} + 9\text{MP} + 1\text{MP}}$ (Radke and Welte, 1983),

$\text{MPI 2} = \frac{3(2\text{MP})}{\text{P} + 9\text{MP} + 1\text{MP}}$ (Radke and Welte, 1983).

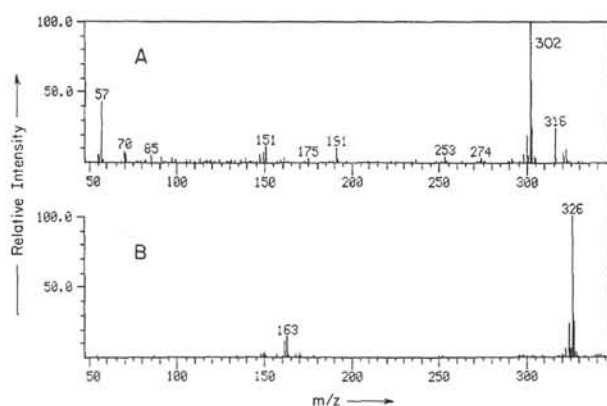


Figure 5. Examples of mass spectra of higher molecular weight PAH $C_{24}H_{14}$ MW 302 (A), for example, dibenzo(a,e)pyrene (I); and $C_{26}H_{14}$ MW 326 (B), various structures.

Phenanthrene is the predominant PAH with successively lesser concentrations of fluoranthene, pyrene, chrysene/triphenylene, benzo-fluoranthenes, benzo(e)pyrene, benzo(a)pyrene, indenopyrene, benzo(ghi)perylene, coronene, and unknowns of molecular weights 302 and 326 (e.g., Fig. 5). There are 65 known compounds with molecular weight (MW) 302 (Lee et al., 1981), and seven compounds with MW 326 which have been assigned structures based on emission and excitation spectra in an extract from carbon black (Peardon et al., 1980). One structural assignment has been made for one of the eight unknowns with MW 302; one analog has the GC retention time of dibenzo(a,e)pyrene (naphtho[1,2,3,4-def]chrysene, Structure I; all chemical structures are given in the Appendix). Possible structural suggestions for the unknown compounds with MW 326 are described by Simoneit (this volume), but confirmation would require authentic standards. This mixture of PAH represents a thermally mature compound assemblage.

The absence of alkanes and dominance of PAH indicate that this nodule precipitated after expulsion of some of the thermally generated alkanes (200°–300°C) and during nodule growth at still elevated temperatures (~150°–200°C) further oxidation of in-situ organic matter occurred to generate PAH. Thus, the high bitumen concentration (Table 2) comprised primarily of PAH is a consequence of entrapment in the carbonate matrix of the nodule of high temperature bitumen (PAH).

Site 858

This site is considered as a currently active hydrothermal discharge zone. Six carbonate concretions recovered at depths ranging from 11.8 to 61.0 mbsf have been analyzed for both stable isotopes and organic matter. The organic matter composition has also been analyzed in the surrounding, less indurated sediment for some concretions.

Nodules

The nodules can be subdivided into two main categories based on the isotopic composition (Früh-Green et al., this volume): those with positive $\delta^{18}O$ /strong negative $\delta^{13}C$ ratios (two samples), and those with variably negative $\delta^{18}O$ /less negative $\delta^{13}C$ ratios (3 samples) (Table 1). Among the first group are the carbonate concretions sampled at shallower depths (the assumed depth of 27.9 mbsf of the nodule 858F-2R-CC, 0–5 cm might correspond to a drilling artifact).

The $\delta^{18}O$ values of the nodule mentioned above and of Sample 858A-2H-7, 40–42 cm (11.8 mbsf) are +2.53‰ and +3.56‰, respectively, while their $\delta^{13}C$ values remain strongly negative (–27.78‰ and –31.79‰, respectively). In these samples the highly ^{18}O -enriched composition of the calcites should indicate low temperatures of for-

mation (Früh-Green et al., this volume), whereas their general sources of carbonate, deduced from the carbon isotopic compositions, as already hypothesized by other authors (Goodfellow and Blaise, 1988; Al-Aasm and Blaise, 1991), can be viewed as the product of a methane-oxidation process (Claypool and Kaplan, 1974; Coleman et al., 1981; Ritger et al., 1987).

Three other nodules (Samples 858A-4H-7, 15–17 cm; 858A-8H-2, 57–59 cm; and 858D-4H-1, 5–7 cm), recovered at 30.6, 61.0, and 19.9 mbsf, respectively, in two different holes, also show fairly depleted values for both $\delta^{18}O$ (variable from –17.08‰ to –5.47‰) and $\delta^{13}C$ (from –9.31‰ to –16.08‰) (Table 1), compared to normal ratios for marine carbonates. The ^{18}O data probably reflect elevated temperatures of carbonate precipitation during diagenesis. The $\delta^{13}C$ values are similar to those measured in the previous sites and indicate a carbonate carbon source from organic matter.

The sixth nodule (Sample 858C-3H-2, 110–115 cm), sampled at 15.5 mbsf, corresponds to a fragment of a sparry calcite breccia, interpreted in the core description (Davis, Mottl, Fisher, et al., 1992) as a dissected fragment from a hydrothermal cap, possibly constraining the lateral flow. Its $\delta^{18}O$ value is –10.70‰, pointing to a temperature of deposition of 77°C, whereas $\delta^{13}C$ reaches –22.76‰, near the thermogenic methane values mentioned for the shallower calcite nodules.

Bitumen

The TC content is significantly higher in the nodules than in the surrounding sediments and the TC of the anhydrite and gypsum breccia is quite low (Table 1). However, some nodules have lower TC contents than other sediments from the same holes (e.g., Sample 857C-36R-1, 50–53 cm, or 858A-2H-7, 40–42 cm, Davis, Mottl, Fisher, et al., 1992). The bitumen yields are significantly lower for the nodules than for the surrounding sediments (Table 2), but within the ranges observed for other sediments in the same holes (Simoneit, this volume; Davis, Mottl, Fisher, et al., 1992).

The *n*-alkanes are present in all samples analyzed from Site 858, although at trace concentrations in some, and they generally range from C_{15} to C_{35} (in one case to C_{39} , cf. Fig. 6A). The CPI values vary over the full maturation range (Table 2) as described for the other sediments from Leg 139 (Simoneit, this volume). They range from 4.9 to 0.62, where full maturity shows a strong even *n*-alkane dominance (Simoneit, this volume). It was proposed that reductive processes acting on *n*-alkanols from marine microbial sources and terrestrial plant waxes (Simoneit, 1977, 1978) may be the source of the even-chain *n*-alkanes, because maturation in these sediments and nodules began with immature organic matter that had not completed diagenesis (Simoneit, this volume). This would require low-temperature alteration by dehydration and double bond reduction of the *n*-alkanols (possibly <100°C) analogous to that described for the alteration of sedimentary organic matter by the intrusives in the Bransfield Strait (Braut and Simoneit, 1988). Further evidence in support of this proposal is discussed by Simoneit (this volume).

In general the CPI is the same for the *n*-alkanes in the nodules and in the respective surrounding sediment, indicating the same thermal maturity. This is also the case for the other hydrocarbon parameters (Table 2). Maturation is not evident in the isoprenoid to normal hydrocarbon ratios ($Pr/n-C_{17}$ and $Ph/n-C_{18}$, Table 2) for these samples, but in general these ratios are relatively low, ranging from 2.1 to 0.19 and from 2.9 to 0.24, respectively (cf. Davis, Mottl, Fisher, et al., 1992). Low $Pr/n-C_{17}$ and $Ph/n-C_{18}$ values (<0.5) are characteristic of basin sediments that are mature (Hunt, 1979). The Pr/Ph ratio ranges from 0.29 to 1.27 for these samples, also showing no trend with maturation.

Biomarkers

The biomarkers occur as trace components only in samples from Holes 858C and 858D. They are comprised of hydrocarbons (Table 2) and not the immature biogenic precursors and intermediates as described for the other sediments from Leg 139 (Simoneit, this volume).

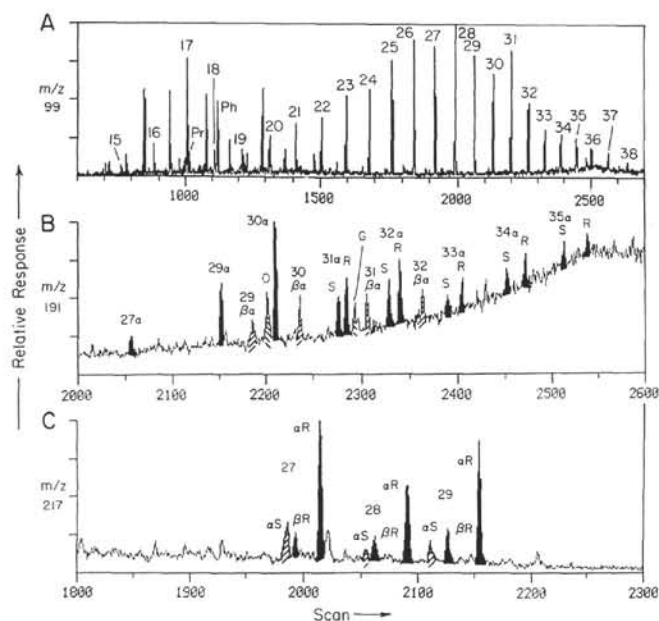


Figure 6. Selected mass fragmentograms for the bitumen from Sample 858D-4H-1, 5–7 cm. **A.** m/z 99, key ion for n -alkanes (numbers refer to carbon chain length, Pr = pristane, Ph = phytane). **B.** m/z 191, key ion for triterpenoids (numbers refer to carbon skeleton size, α = $17\alpha(\text{H}), 21\beta(\text{H})$ -hopane configuration, $\beta\alpha$ = $17\beta(\text{H}), 21\alpha(\text{H})$ configuration, S and R = configuration at C-22, O = oleanane, G = gammacerane). **C.** m/z 217, key ion for steranes (numbers refer to carbon skeleton size, α = $5\alpha(\text{H}), 14\alpha(\text{H}), 17\alpha(\text{H})$ configuration, S and R = configuration at C-20).

Hopanes undergo maturation under hydrothermal conditions from immature precursors, including the $17\beta(\text{H}), 21\beta(\text{H})$ -hopanes (II) and moretanes [$17\beta(\text{H}), 21\alpha(\text{H})$ -hopanes, III], to the $17\alpha(\text{H}), 21\beta(\text{H})$ -hopanes (IV). The configuration of the biological precursors is $17\beta(\text{H}), 21\beta(\text{H})$ for this series as the R epimer at C-22 for the extended homologs $>C_{31}$ (Ensminger et al., 1974, 1977). Maturation converts the precursors to the thermodynamically most stable configuration of $17\alpha(\text{H}), 21\beta(\text{H})$, with the S and R epimers at C-22 for the extended homologs $>C_{31}$ at an equilibrium ratio

$$\left(\frac{S}{S+R}\right)$$

of about 0.6 (Ensminger et al., 1974, 1977; Seifert and Moldowan, 1978). Typical examples for this series are shown in Figures 6 and 7, and the maturity parameters are given in Table 2. The hopanes in these samples range from C_{27} to C_{35} , with C_{30} predominant and primarily the $17\alpha(\text{H}), 21\beta(\text{H})$ configuration. Significant amounts of $18\alpha/\beta(\text{H})$ -oleanane (V) and gammacerane (VI) are present. This same pattern is also observed for other sediments from Leg 139 (Simoneit, this volume). The lowest maturity is found in Sample 858C-2H-5, 71–73 cm (nodule and sediment) and full maturity only 5 m deeper in Sample 858C-3H-2, 110–115 cm (Table 2). Both nodules and surrounding sediments have the same hopane maturities.

Sterane hydrocarbons, useful for oil-source rock and maturity comparisons (Mackenzie et al., 1982; Seifert and Moldowan, 1978), also exhibit differences among these samples. Examples of the sterane maturation in this limited sample suite are given in Figures 6C and 8 and the parameter data are listed in Table 2. The steranes have distributions with C_{27} dominant, with C_{28} and C_{29} as intermediate and C_{30} as a minor component. Sample 858D-4H-1, 5–7 cm, contains significant concentrations of C_{27} to C_{29} steranes (VII), primarily with the $5\alpha(\text{H}), 14\alpha(\text{H}), 17\alpha(\text{H})$ -20R and less of the 20S configurations, and smaller

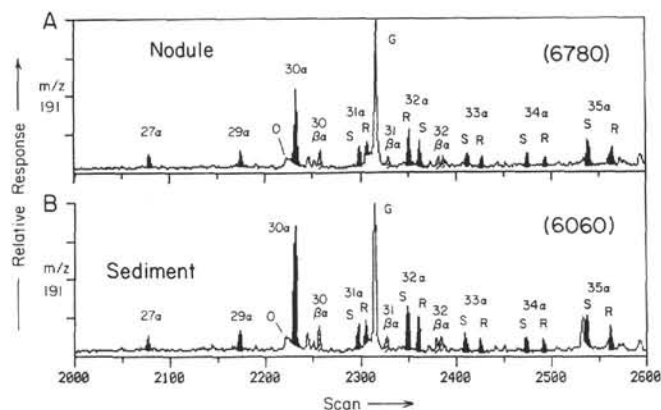


Figure 7. Mass fragmentograms of m/z 191 for Sample 858C-3H-2, 110–115 cm, nodule (A) and sediment (B). Numbers and symbols as in Figure 6B.

amounts of the thermally less stable $5\beta(\text{H}), 14\alpha(\text{H}), 17\alpha(\text{H})$ -20R configuration (Fig. 6C, cf. Kawka and Simoneit, 1987). Sample 858C-3H-2, 110–115 cm (Fig. 8), exhibits essentially complete epimerization at C-20 as occurs during thermal maturation (Seifert and Moldowan, 1978; Mackenzie et al., 1980). The epimerization ratio at C-20,

$$\left(\frac{20S}{20S+20R}\right)$$

of C_{29} , is 0.40 for these two samples (Table 2) with full maturity representing a C_{29} epimerization ratio of 0.45. The epimerization ratio for the nodule Sample 858D-4H-1, 5–7 cm, is 0.15, quite immature. This sample consists of a considerable amount of drilling rubble and thus represents a mixture of components from shallower depths, that is, less mature. Higher sterane maturities result in additional isomerization as is evident by the presence of the $5\alpha(\text{H}), 14\beta(\text{H}), 17\beta(\text{H})$ -20R and 20S-steranes (VIII, e.g., Fig. 8B, -D) and an increase of the diasteranes [IX, $13\beta(\text{H}), 17\alpha(\text{H})$ -20S/R] relative to the steranes. These sterane compositions are analogous to those reported earlier for shallow samples from the hydrothermal vent area near Site 858 (Simoneit et al., 1992) and for the other Leg 139 sediments (Simoneit, this volume). The maturation also parallels the data for hydrothermal petroleum from Guaymas Basin and Escanaba Trough (Kawka and Simoneit, 1987; Kvenvolden and Simoneit, 1990; Simoneit, 1985). The sterane distributions and maturity are the same within the nodules as in the surrounding sediments. The conversion of the natural product precursors of the biomarkers to their mature geological derivatives (cf. Simoneit, this volume) requires strong reducing conditions during hydrothermal alteration.

One sample set, 858C-3H-2, 110–115 cm, nodule and sediment, had trace amounts of C_{37} methylalka-dien- and -trien-ones (Fig. 9). These compounds are ubiquitous in the shallower, thermally unaltered sediments of Middle Valley and are degraded to unknown products by hydrothermal fluids $>200^\circ\text{C}$ (Simoneit et al., this volume). Sample 858C-3H-2, 110–115 cm, has experienced temperatures in this range and the others with no alkenones were probably at higher temperatures or at similar temperatures for longer time periods.

Polynuclear Aromatic Hydrocarbons

The low molecular weight aromatic and alkyl aromatic hydrocarbons are preserved in the nodules (Table 3) unlike in the sediments from this area (Simoneit, this volume). Thus, phenanthrene and alkyl phenanthrenes are present at significant concentrations in these nodule samples (Fig. 3), which indicates that the PAH were trapped and/or introduced into the nodules during their growth by aqueous fluids and the lower molecular weight aromatics were thus retained. The

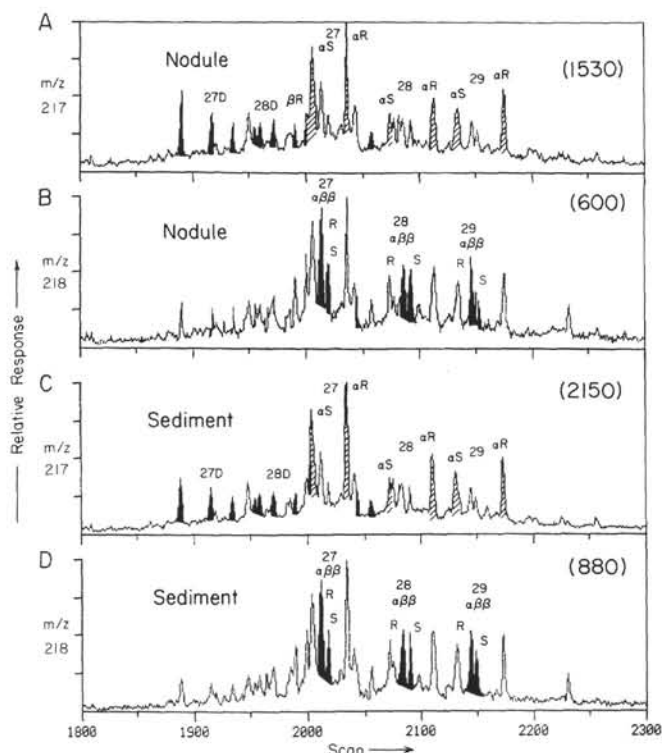


Figure 8. Mass fragmentograms of m/z 217 and 218 for the bitumen in the nodule (A, B) and sediment (C, D) of Sample 858C-3H-2, 110–115 cm. Numbers and symbols as in Figure 6C. D = diasteranes, $\alpha\beta\beta$ = $5\alpha(H), 14\beta(H), 17\beta(H)$ configuration).

ranges of the phenanthrene to methylphenanthrenes (P/MP) ratio are 0.36 to 15.0, MPI 1 = 0.05–2.35, and MPI 2 = 0.05–2.82 (methyl phenanthrene index calculated according to Radke and Welte, 1983; Table 3). These ranges represent mature to overmature phenanthrene distributions. The higher alkyl phenanthrene homologs are present at typically decreasing concentrations as observed for other hydrothermal petroleum and the indices are also similar (Kawka and Simoneit, 1990; Kvenvolden and Simoneit, 1990).

Another trend observed in the PAH distributions from semi-mature to mature samples (cf. Figs. 3, 4, and 10) is the disappearance of perylene vs. benzofluoranthenes and benzopyrenes (from a ratio of 35 to 0.01, Table 3). This is the mature portion of the trend as described for other samples from Leg 139 (Simoneit, this volume), and for Guaymas Basin sediments and hydrothermal petroleum (Baker and Louda, 1982; Simoneit and Philp, 1982; Simoneit et al., 1984; Kawka and Simoneit, 1990). Perylene is generated by diagenetic processes at depth but is not stable at catagenetic temperatures (Louda and Baker, 1984; Kawka and Simoneit, 1990).

A further observation reflects the aqueous solubility of the lower molecular weight PAH resulting in preferential concentration of the remaining higher weight PAH. This trend is illustrated in Figure 3A–C by the depletion of phenanthrene followed by fluoranthene and pyrene, and in Figure 4A, -B vs. 4C by the depletion of the m/z 252 cluster of benzofluoranthenes, benzo(a)pyrene, and benzo(e)pyrene (BaP and BeP, respectively).

Fluoranthene and pyrene occur with variable ratios (fluoranthene/pyrene range 0.10 to 1.13, Figs. 4 and 10, Table 3). Significant concentrations of the benzopyrenes are present in these samples (Figs. 4 and 10). The ratio of BaP/BeP (Table 3) can be used to gauge the extent of secondary oxidation of the PAH once formed, because BaP is less stable than BeP (Lane, 1989; Nielsen et al., 1984). The BaP/BeP range for these samples is from 0.03 to 0.47 (Table 3), in which

a typical precursor value is >0.4 and those samples with a ratio <0.4 have had an oxidative or thermal loss of BaP. The ratio of coronene to the total benzofluoranthenes plus BeP plus BaP (Table 3) reflects the content of PAH with higher molecular weights and ranges from 0.07 to 2.18. Thus, Samples 858C-3H-2, 110–115 cm, and 858C-2H-5, 71–73 cm, have the highest concentrations of PAH $> m/z$ 300 and also suffered significant secondary PAH oxidation and removal due to extensive fluid washing. In general, the PAH distributions are the same in the bitumen from the nodules and their respective surrounding sediments (e.g., Fig. 10), indicating the bitumen was trapped and diluted by the ingrowth of the nodule.

The high temperatures ($>300^\circ\text{C}$) required for PAH formation indicate that fluids in that temperature window with the PAH passed through these sediments, in turn cracking the in-situ organic matter to hydrothermal petroleum (i.e., aliphatic hydrocarbons), migrating the oil onward, and leaving behind the PAH. Subsequent or concurrent nodule precipitation occurred from CO_2 in the fluids, where the former retained primarily the high molecular weight PAH and the latter entrapped low to high molecular weight PAH.

CONCLUSIONS

There are three types of isotopically distinct nodules (Fig. 11):

1. Nodules formed from CO_2 derived by microbial methane oxidation during sedimentary diagenesis in shallow sections (type I). They have more positive $\delta^{18}\text{O}$ values and light $\delta^{13}\text{C}$ values.
2. Nodules precipitated with CO_2 derived from oxidation reactions of organic matter by sulfate resulting in lighter $\delta^{18}\text{O}$ values and heavier $\delta^{13}\text{C}$ values. They occur at various depths, generally below 10 mbsf, during late diagenesis (type II). Calcite from a hydrothermal cap consisting of brecciated sediment (Sample 858C-3H-2, 110–115 cm) also fits within type II.
3. Nodules and sediment affected by high-temperature fluids (type III), with CO_2 derived from catagenetic sources and from organic matter oxidation by sulfate.

The sources of the carbonates are compared with the corresponding bitumen types in Table 4. The bitumen types reflect a maturity consistent with the temperatures calculated from the $\delta^{18}\text{O}$ of the carbonates, assuming an altered oxygen isotope composition of the hydrothermal fluid of 2‰ (SMOW). The bitumen concentrations are less in the nodules than in their surrounding sediments for all examples studied. However, the compositions and all the maturity parameters are essentially the same for each nodule and its respective sediment. This indicates that the nodules grew during active fluid migration through the sediments, after organic matter alteration at high temperatures ($>250^\circ\text{C}$), resulting in carbonate precipitation that diluted the mineral matrix and associated organic matter. This process also removed water-soluble matter and early generated bitumen in some cases and in others all hydrothermal organic products were trapped. The presence of dominantly PAH reflects the high fluid temperature either prior to or during carbonate precipitation. The calculated temperature ($\delta^{18}\text{O}$) is the more realistic in-situ temperature during carbonate nodule growth. Sample 858C-3H-2, 110–115 cm (nodule type II), has the highest bitumen yield of this study. Its bitumen composition and maturity are typical of hydrothermal petroleum from Middle Valley, supporting the interpretation that this calcite is derived from a hydrothermal cap. Sample 857C-36R-1, 50–53 cm, from 346.5 mbsf, also has a high bitumen yield. This bitumen is composed primarily of PAH from phenanthrene (quite water soluble) to high molecular weight PAH, indicating carbonate growth from fluids at high temperature and enriched in CO_2 and PAH. As precipitation progressed, all PAH were entrapped. The conversions of immature natural product precursors of biomarkers to their mature geological derivatives requires strong reducing conditions during hydrothermal alteration.

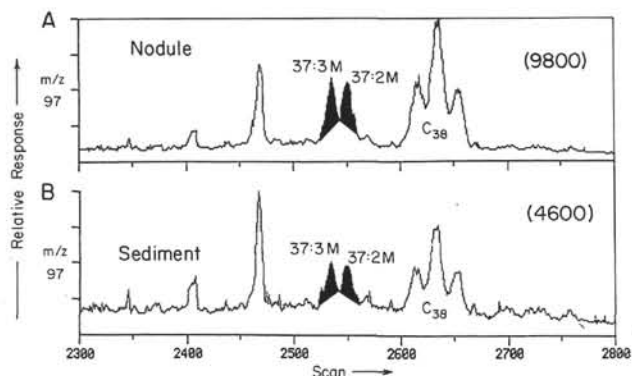


Figure 9. Mass fragmentograms for m/z 97, key ion for alkenones in Sample 858C-3H-2, 110–115 cm, nodule (A) and sediment (B) (37:3M = C_{37} alkatrien-2-one, 37:2M = C_{37} alkadien-2-one, C_{38} = C_{38} alkenones).

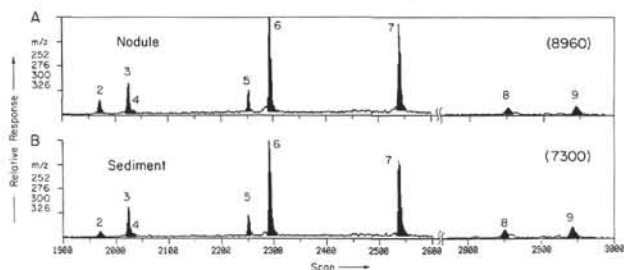


Figure 10. Summed mass fragmentograms (m/z 252, 276, 300, 326) for selected PAH in total bitumen of Sample 858C-3H-2, 110–115, nodule (A) and sediment (B). Numbers refer to compounds in Figure 4.

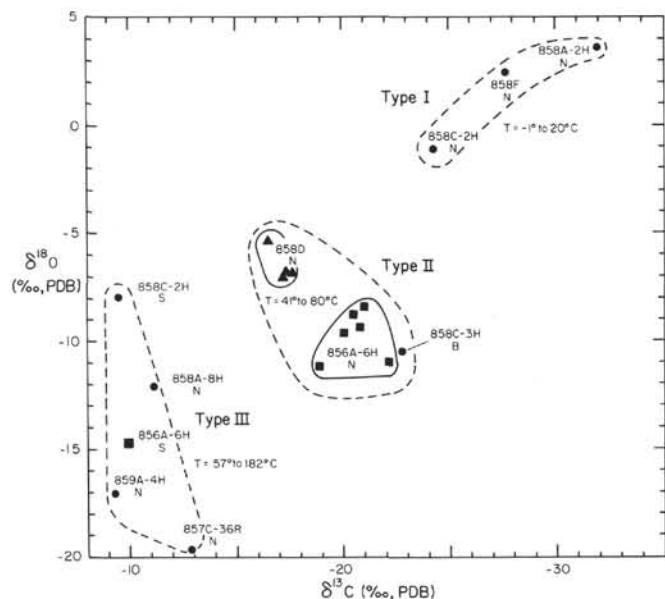


Figure 11. Correlation diagram of $\delta^{13}C$ vs. $\delta^{18}O$ of the samples analyzed here, showing the clustering into three types (N = nodule, S = sediment).

ACKNOWLEDGMENTS

Financial support (Boni) from CNR (Grants A.I.05.9205478 and CTB 1993–M.B. Cita to M.B.) and (BRTS) from the National Science Foundation, Division of Ocean Sciences (Grant OCE-9002366), and from the NSF and JOI, Inc., U.S. Science Support Program of the

Ocean Drilling Program is gratefully acknowledged. We thank Baiyun Ran for technical assistance.

The U.S. Science Program associated with the Ocean Drilling Program is sponsored by the National Science Foundation and the Joint Oceanographic Institutions, Inc. Any opinions, findings, and conclusions or recommendations expressed in this publication are those of the author and do not necessarily reflect the views of the National Science Foundation, the Joint Oceanographic Institutions, Inc., or Texas A&M University.

REFERENCES*

- Al-Aasm, I.S., and Blaise, B., 1991. Interaction between hemipelagic sediment and a hydrothermal system: Middle Valley, northern Juan de Fuca Ridge, subarctic northeast Pacific. *Mar. Geol.*, 98:25–40.
- Baker, E.W., and Louda, J.W., 1982. Geochemistry of tetrapyrrole, tetraterpenoid, and perylene pigments in sediments from the Gulf of California: Deep Sea Drilling Project Leg 64, Sites 474, 477, 479, and 481, and Scripps Institution of Oceanography Guaymas Basin Survey Cruise Leg 3, Sites 10G and 18G. In Curray, J.R., Moore, D.G., et al., *Init. Repts. DSDP*, 64 (Pt. 2): Washington (U.S. Govt. Printing Office), 789–814.
- Blumer, M., 1975. Curtisite, idrialite and pendletonite, polycyclic aromatic hydrocarbon minerals: their composition and origin. *Chem. Geol.*, 16:245–256.
- Brault, M., and Simoneit, B.R.T., 1988. Steroid and triterpenoid distributions in Bransfield Strait sediments: hydrothermally-enhanced diagenetic transformations. In Mattavelli, L., and Novelli, L. (Eds.), *Advances in Organic Geochemistry 1987*, 13:697–705.
- Claypool, G.E., and Kaplan, I.R., 1974. The origin and distribution of methane in marine sediments. In Kaplan, I.R. (Ed.), *Natural Gases in Marine Sediments*: New York (Plenum), 99–139.
- Coleman, M.L., Risatti, J.B., and Schoell, M., 1981. Fractionation of carbon and hydrogen isotopes by methane-oxidizing bacteria. *Geochim. Cosmoch. Acta*, 45:1033–1037.
- Davis, E.E., Currie, R.G., and Kosalos, J.G., 1987. Marine geophysical maps of western Canada: regional Sea MARC II acoustic image mosaics and Sea Beam bathymetry. *Geol. Surv. Can.*, Maps 2-1987-17-1987.
- Davis, E.E., Goodfellow, W.D., Bornhold, B.D., Adshead, J., Blaise, B., Villinger, H., and Le Cheminant, G.M., 1987. Massive sulfides in a sedimented rift valley, northern Juan de Fuca Ridge. *Earth Planet. Sci. Lett.*, 82:49–61.
- Davis, E.E., Mottl, M.J., Fisher, A.T., et al., 1992. *Proc. ODP, Init. Repts.*, 139: College Station, TX (Ocean Drilling Program).
- Davis, E.E., and Villinger, H., 1992. Tectonic and thermal structure of the Middle Valley sedimented rift, northern Juan de Fuca Ridge. In Davis, E.E., Mottl, M.J., Fisher, A.T., et al., *Proc. ODP, Init. Repts.*, 139: College Station, TX (Ocean Drilling Program), 9–41.
- Ensminger, A., Albrecht, P., Ourisson, G., and Tissot, B., 1977. Evolution of polycyclic alkanes under the effect of burial (Early Toarcian Shales, Paris Basin). In Campos, R., and Goni, J. (Eds.), *Advances in Organic Geochemistry 1975*: Madrid (ENADIMSA), 45–52.
- Ensminger, A., van Dorsselaer, A., Spyckerelle, C., Albrecht, P., and Ourisson, G., 1974. Pentacyclic triterpenes of the hopane type as ubiquitous geochemical markers: origin and significance. In Tissot, B., and Biener, F. (Eds.), *Advances in Organic Geochemistry 1973*: Paris (Editions Technip), 245–260.
- Friedman, I., and O'Neil, J., 1977. Compilation of stable isotope fractionation factors of geochemical interest. In Fleischer, M. (Ed.), *Data of Geochemistry* (6th Ed.). Geol. Surv. Prof. Pap. U.S., 440-KK:1–12.
- Goodfellow, W.D., and Blaise, B., 1988. Sulphide formation and hydrothermal alteration of hemipelagic sediment in Middle Valley, northern Juan de Fuca Ridge. *Can. Mineral.*, 26:675–696.
- Hunt, J.M., 1979. *Petroleum Geochemistry and Geology*: San Francisco (W.H. Freeman).
- Kawka, O.E., and Simoneit, B.R.T., 1987. Survey of hydrothermally-generated petroleum from the Guaymas Basin spreading center. *Org. Geochem.*, 11:311–328.
- , 1990. Polycyclic aromatic hydrocarbons in hydrothermal petroleum from the Guaymas Basin spreading center. In Simoneit, B.R.T. (Ed.),

* Abbreviations for names of organizations and publications in ODP reference lists follow the style given in *Chemical Abstracts Service Source Index* (published by American Chemical Society).

- Organic Matter in Hydrothermal Systems—Petroleum Generation, Migration and Biogeochemistry*. Appl. Geochem., 5:17–27.
- Kvenvolden, K.A., and Simoneit, B.R.T., 1990. Hydrothermally derived petroleum: examples from Guaymas Basin, Gulf of California and Escanaba Trough, Northeast Pacific Ocean. *AAPG Bull.*, 74:223–237.
- Lane, D.A., 1989. The fate of polycyclic aromatic compounds in the atmosphere and during sampling. In Vo-Dinh, T. (Ed.), *Chemical Analysis of Polycyclic Aromatic Compounds*. Chem. Anal., 101:31–58.
- Lee, M.L., Novotny, M.V., and Bartle, K.D., 1981. *Analytical Chemistry of Polycyclic Aromatic Compounds*: New York (Academic Press), 376–386.
- Louda, J.W., and Baker, E.W., 1984. Perylene occurrence and possible sources in deep-ocean sediments. *Geochim. Cosmochim. Acta*, 48:1043–1058.
- Machel, H.G., 1987. Some aspects of diagenetic sulphate-hydrocarbon redox reactions. In Marshall, J.D. (Ed.), *Diagenesis of Sedimentary Sequences*. Geol. Soc. Spec. Publ. London, 36:15–28.
- Mackenzie, A.S., Brassell, S.C., Eglinton, G., and Maxwell, J.R., 1982. Chemical fossils: the geological fate of steroids. *Science*, 217:491–504.
- Mackenzie, A.S., Patience, R.L., Maxwell, J.R., Vandenbroucke, M., and Durand, B., 1980. Molecular parameters of maturation in the Toarcian shales, Paris Basin, France—I. Changes in the configurations of acyclic isoprenoid alkanes, steranes and triterpanes. *Geochim. Cosmochim. Acta*, 44:1709–1721.
- McCrea, J.M., 1950. Isotopic chemistry of carbonates and a paleotemperature scale. *J. Chem. Phys.*, 18:849–857.
- Nielsen, T., Seitz, B., and Ramdahl, T., 1984. Occurrence of nitro-PAH in the atmosphere in a rural area. *Atmos. Environ.*, 18:2159–2165.
- Peardon, P.A., Lee, M.L., Hirata, Y., and Novotny, M., 1980. High-performance liquid chromatographic separation of high-molecular-weight polycyclic aromatic compounds in carbon black. *Anal. Chem.*, 52:2268–2271.
- Radke, M., and Welte, D.H., 1983. The Methylphenanthrene Index (MPI): a maturity parameter based on aromatic hydrocarbons. In Bjørøy, M., et al. (Eds.), *Advances in Organic Geochemistry 1981*: Chichester (Wiley), 504–512.
- Raiswell, R., 1987. Non-steady state microbiological diagenesis and the origin of concretions and nodular limestones. In Marshall, J.D. (Ed.), *Diagenesis of Sedimentary Sequences*. Geol. Soc. Spec. Publ. London, 36:41–54.
- Ritger, S., Carson, B., and Suess, E., 1987. Methane-derived authigenic carbonates formed by subduction-induced pore water expulsion along the Oregon/Washington margin. *Geol. Soc. Am. Bull.*, 98:147–156.
- Scott, L.T., 1982. Thermal rearrangements of aromatic compounds. *Acc. Chem. Res.*, 15:52–58.
- Seifert, W.K., and Moldowan, J.M., 1978. Applications of steranes, terpanes and monoaromatics to the maturation, migration and source of crude oils. *Geochim. Cosmochim. Acta*, 42:77–95.
- Sharma, T., and Clayton, R.N., 1965. Measurement of $^{18}\text{O}/^{16}\text{O}$ ratios of total oxygen in carbonates. *Geochim. Cosmochim. Acta*, 29:1347–1353.
- Simoneit, B.R.T., 1977. Diterpenoid compounds and other lipids in deep-sea sediments and their geochemical significance. *Geochim. Cosmochim. Acta*, 41:463–476.
- , 1978. The organic chemistry of marine sediments. In Riley, J.P., and Chester, R. (Eds.), *Chemical Oceanography* (2nd ed.) (Vol. 7): New York (Academic Press), 233–311.
- , 1984. Hydrothermal effects on organic matter—high versus low temperature components. In Schenck, P.A., deLeeuw, J.W., and Lijmbach, G.W.M. (Eds.), *Advances in Organic Geochemistry 1983*: Oxford (Pergamon Press), *Org. Geochem.*, 6:857–864.
- , 1985. Hydrothermal petroleum: genesis, migration and deposition in Guaymas Basin, Gulf of California. *Can. J. Earth Sci.*, 22:1919–1929.
- Simoneit, B.R.T., Goodfellow, W.D., and Franklin, J.M., 1992. Hydrothermal petroleum at the seafloor and organic matter alteration in sediments of Middle Valley, northern Juan de Fuca Ridge. *Appl. Geochem.*, 7:257–264.
- Simoneit, B.R.T., and Lonsdale, P.F., 1982. Hydrothermal petroleum in mineralized mounds at the seabed of Guaymas Basin. *Nature*, 295:198–202.
- Simoneit, B.R.T., and Philp, R.P., 1982. Organic geochemistry of lipids and kerogen and the effects of basalt intrusions on unconsolidated oceanic sediments: Sites 477, 478, and 481, Guaymas Basin, Gulf of California. In Curran, J.M., Moore, D.G., et al., *Init. Repts. DSDP*, 64 (Pt. 2): Washington (U.S. Govt. Printing Office), 883–904.
- Simoneit, B.R.T., Philp, R.P., Jenden, P.D., and Galimov, E.M., 1984. Organic geochemistry of Deep Sea Drilling Project sediments from the Gulf of California – hydrothermal effects on unconsolidated diatom ooze. *Org. Geochem.*, 7:173–205.

Date of initial receipt: 29 March 1993

Date of acceptance: 30 August 1993

Ms 139SR-235

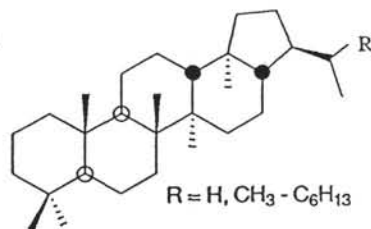
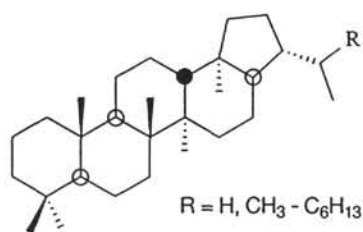
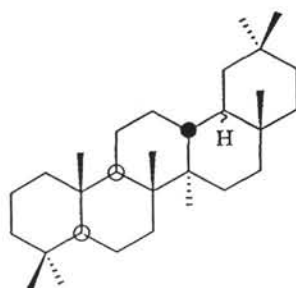
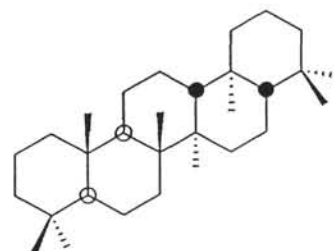
Table 4. Summary comparison of carbonates with bitumen type.

Sample	CO ₂ source	Carbonate		Bitumen type
		Temp. calc. (°C)		
Type I (cf., Fig. 11)		<u>a</u>	<u>b</u>	
858A-2H-7, 40-42	Microbial CH ₄ oxidation	-1	7	Immature (background)
858C-2H-5, 71-73	Microbial CH ₄ oxidation	20	29	Immature, minor influx PAH
858F-2R-CC, 0-5	Microbial CH ₄ oxidation	3	11	—
Type II				
856A-6H-4, 73-76	Microbial and thermochemical organic matter oxidation	68	84	Mature
858C-3H-2, 110-115	Thermochemical organic matter oxidation	77	93	Mature (washed)
858D-4H-1, 5-7	Microbial and thermochemical organic matter oxidation	50	63	Mature
Type III				
856A-6H-4, 18-22(s)	Thermochemical organic matter oxidation	114	137	Overmature
857C-36R-1, 50-53	Thermochemical and catagenetic	182	220	Overmature
858A-4H-7, 15-17	Thermochemical and catagenetic	142	170	Overmature
858A-8H-2, 57-59	Thermochemical organic matter oxidation	88	106	Mature
858C-2H-5, 71-73(s)	Thermochemical organic matter oxidation	57	70	Mature (washed)

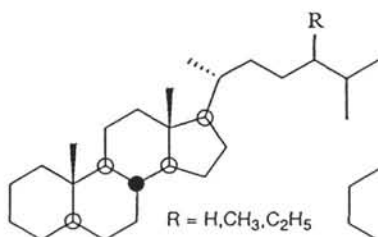
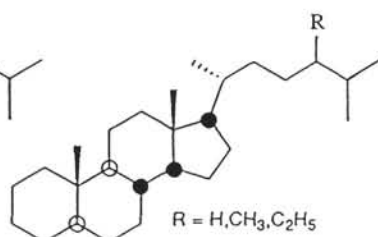
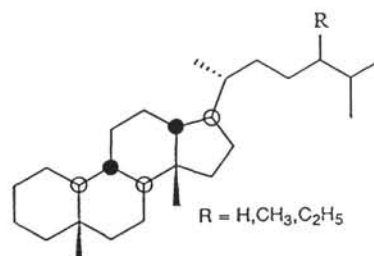
¹ a from $\delta^{18}\text{O}_{\text{H}_2\text{O}} = 0\text{‰}$, b from $\delta^{18}\text{O}_{\text{H}_2\text{O}} = 2\text{‰}$, see footnote in Table 1.
s = sediment

APPENDIX

Chemical Structures Cited

I. Dibenzo(a,e)pyrene $C_{24}H_{14}$ II. $17\beta(H),21\beta(H)$ -HopanesIII. $17\beta(H),21\alpha(H)$ -HopanesIV. $17\alpha(H),21\beta(H)$ -HopanesV. $18\alpha/\beta(H)$ -Oleanane

VI. Gammacerane

VII. $5\alpha(H),14\alpha(H),17\alpha(H)$ -SteranesVIII. $5\alpha(H),14\beta(H),17\beta(H)$ -SteranesIX. $10\alpha(H),13\beta(H),17\alpha(H)$ -Diasteranes